Electronic Supplementary Material (ESI) for Nanoscale.

Supporting Information

Manipulation of the Crystalline Phase Diagram of Hydrogen through Nanoscale Confinement Effects in Porous Carbons

Lui R. Terry[†], Stephane Rols[‖], Mi Tian[‡], Ivan da Silva[§], Simon J. Bending[¶], Valeska P. Ting[†]**

Table S1. Average surface area and pore volume characteristics of powdered acid-washed TE7 and OLC samples

Sample	**Surface Area (m²/g)**			**Pore Volume (cm³/g)**	
	SA_{BET}	SA_{micro}[c]	$SA_{N2CO2\text{-}DFT}$[d]	V_{tot}[e]	$V_{N2CO2\text{-}DFT}$[f]
TE7	1391 ±90[a]	1130 ±90	1316	0.776 ±0.041	0.584
OLC	315 ±1[b]	14 ±2	229	0.904 ±0.030	0.770

[a] Calculated from Rouqerol BET method applied to N_2 adsorption data at 77 K for $0.007 < P/P_0 < 0.05$

[b] Calculated from Rouqerol BET method applied to N_2 adsorption data at 77 K for $0.05 < P/P_0 < 0.3$

[c] Micropore surface area calculated from the statistical t-method using carbon black STSA model thickness range 3.3 – 5.5 Å

[d] Maximum Surface area in pores ≥ 3.3 Å calculated with combined N_2 and CO_2 advanced NLDFT

[e] Single point pore volume corresponding to p/p^o 0.94

[f] Maximum pore volume of pore sizes < 200 Å calculated with combined N_2 and CO_2 advanced NLDFT

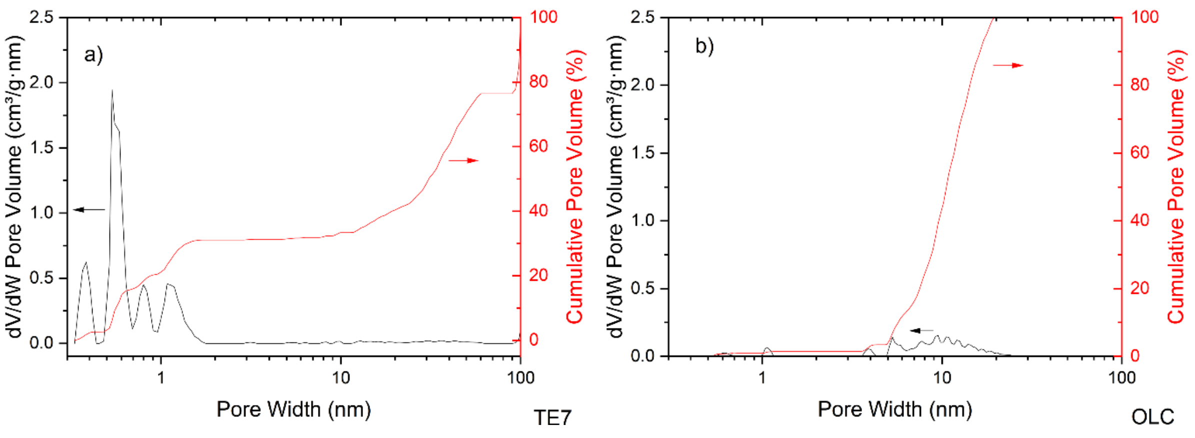

Figure S1: Average pore size distributions of activated carbons (a) microporous TE7 and (b) mesoporous OLC. Calculated by advanced N2-CO2 NL-DFT activated carbon slit-like pore model.

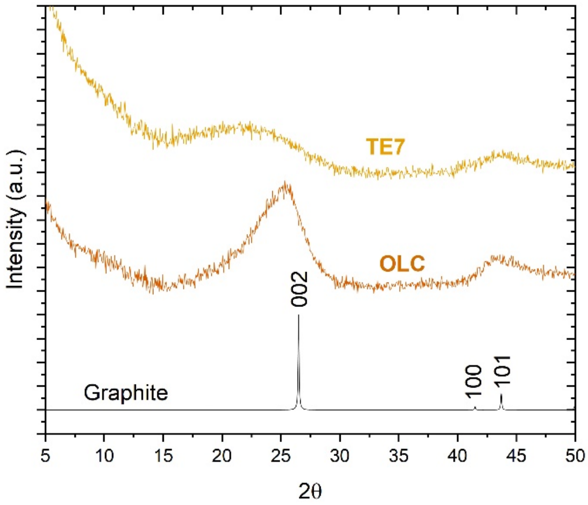

Figure S2. Powder X-ray diffraction patterns of porous carbons OLC and TE7 exhibiting a certain degree of amorphicity compared to graphite[7] , offset in the y-direction, for clarity.

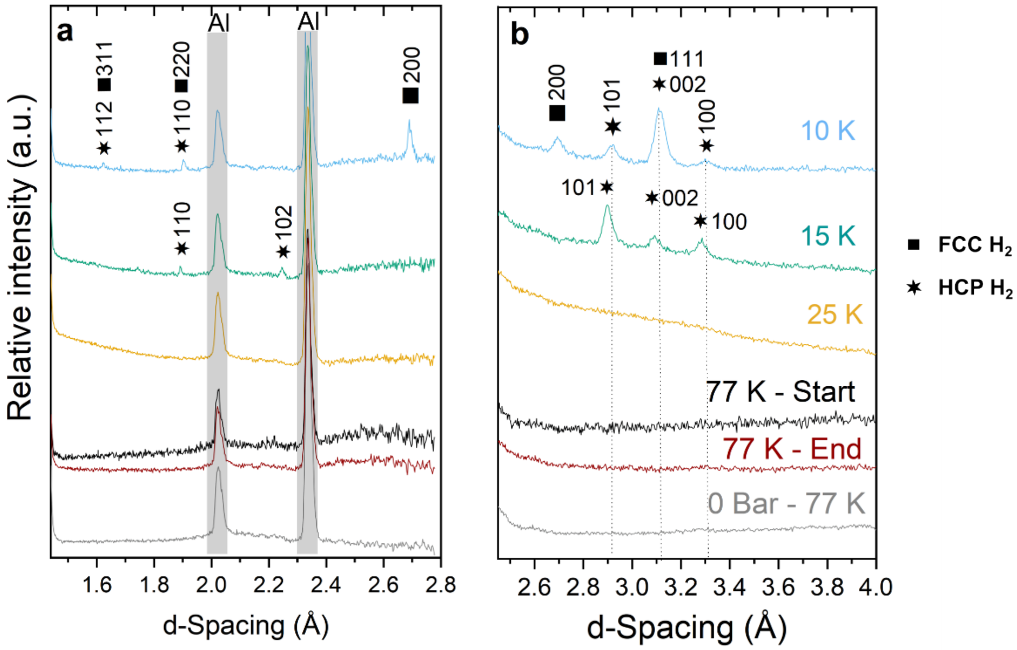

Figure S3. Temperature-dependent neutron powder diffraction for microporous TE7 dosed to 200 bar H_2 at 77 K. Neutron diffraction data from detector bank 5 (a) and bank 3 (b) of the GEM diffractometer, respectively. Stars represent reflections for a solid H_2 HCP phase, filled squares represent reflections for a solid H_2 FCC phase. Reflections from the aluminium cell are shaded in grey and patterns offset in the y-direction for clarity. Dotted lines are added as a guide to the eye to show the HCP unit cell getting smaller with increasing temperature (negative thermal expansion).

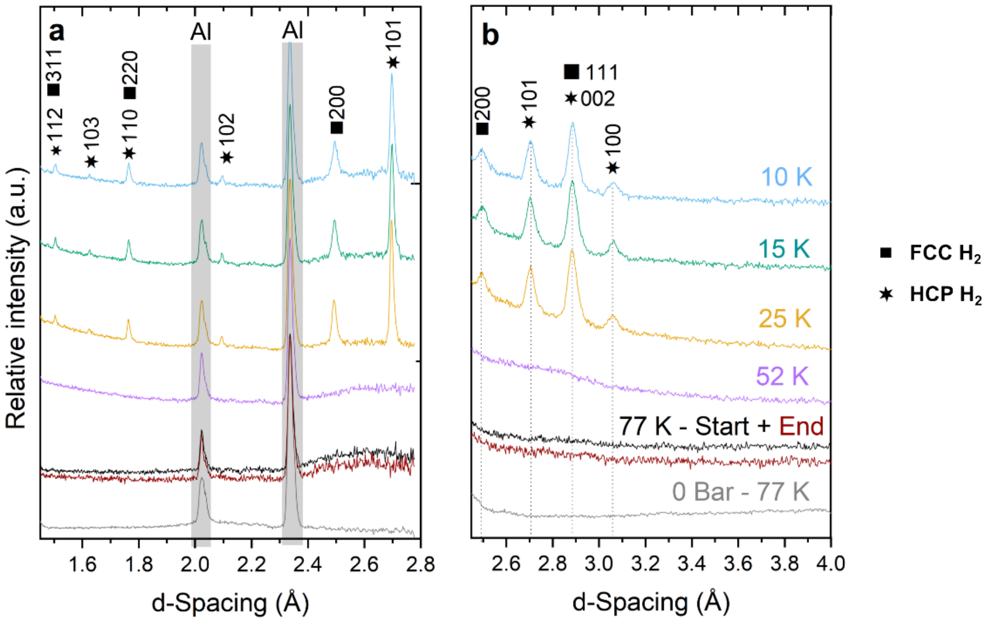

Figure S4. Temperature-dependent neutron powder diffraction data for microporous TE7 dosed to 2 kbar H_2 at 77 K. Neutron diffraction data from detector bank 5 (a) and bank 3 (b) of the GEM diffractometer, respectively. Stars represent reflections for a solid H_2 HCP phase, filled squares represent reflections for a solid H_2 FCC phase. Reflections from the aluminium cell are shaded in grey. Patterns offset in the y-direction, for clarity. Dotted lines are added as a guide to the eye to show insignificant change to unit cell dimensions with temperature.

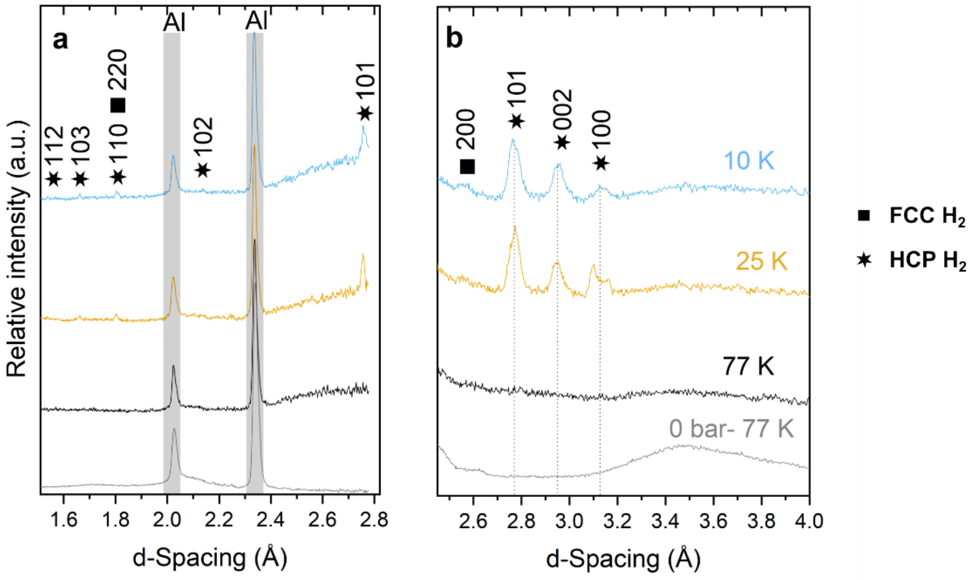

Figure S5. Temperature-dependent elastic neutron diffraction data for mesoporous OLC dosed to 2 kbar H_2 at 77 K. Neutron diffraction data from detector bank 5 (a) and bank 3 (b) of the GEM diffractometer, respectively. Stars represent reflections for a solid H_2 HCP phase. Reflections from the aluminium cell are shaded in grey. Patterns offset in the y-direction, for clarity. Dotted lines are added as a guide to the eye to show unit cell dimension show insignificant change with temperature.

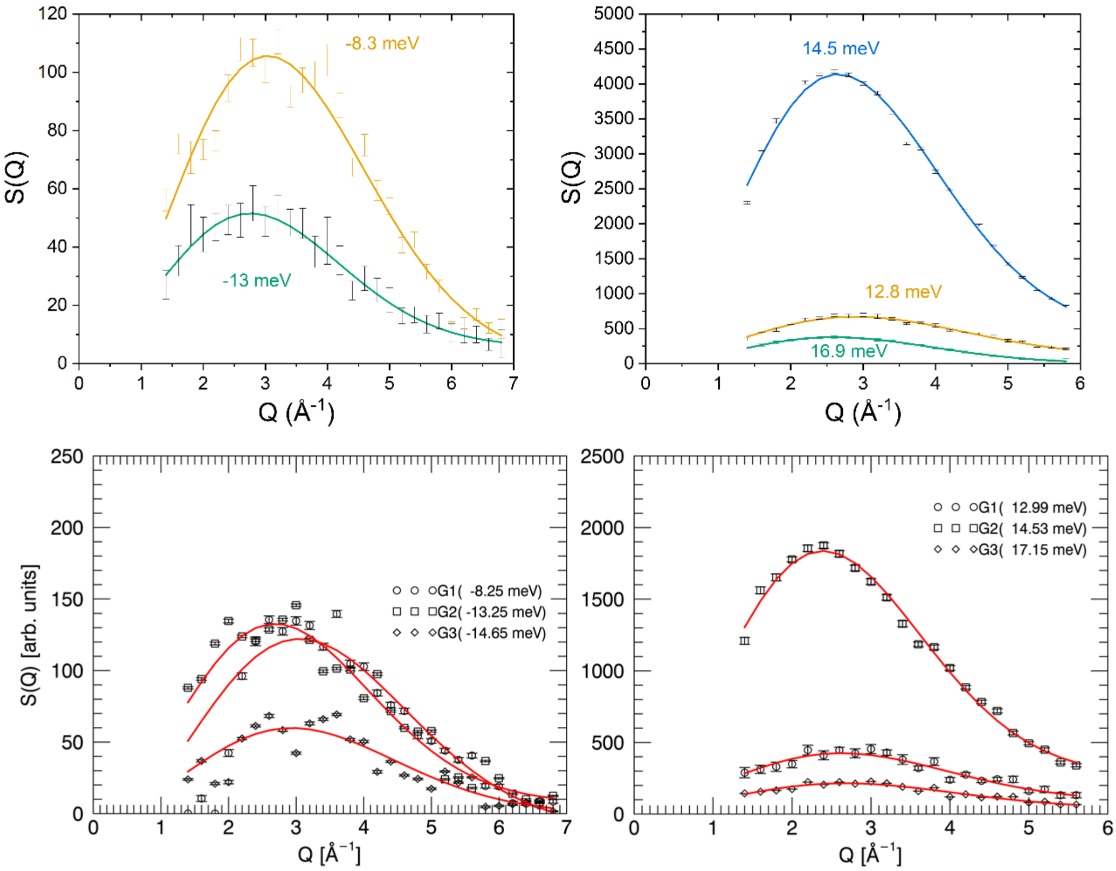

Figure S6: The Q dependence of $J = 0 \rightarrow 1$ and $J = 1 \rightarrow 0$ rotational transition peak contributions at 4 K and 40 K, fitted to solve for U^2 where

$$S(Q) = \exp\left(-\frac{Q^2U^2}{3}\right) * \left[j_1\left(\frac{Qa}{2}\right)\right]^2;\ a = 0.74\ \text{Å}$$

Table S2. Observed *d*-spacings and associated crystal system miller indices for each H_2 dosed activated carbon at 10 K.

TE7 – 200 bar H_2			TE7 – 2 kbar H_2			OLC – 2 kbar H_2		
d-spacing (Å)	HCP - *hkl*	FCC - *hkl*	*d*-spacing (Å)	HCP - *hkl*	FCC - *hkl*	*d*-spacing (Å)	HCP - *hkl*	FCC - *hkl*
1.622	112	311	1.505	112	311	1.662	103	-
1.902	110	220	1.625	103	-	1.804	110	220
2.690	-	200	1.764	110	220	2.546	-	200
2.923	101	-	2.097	102	-	2.756	101	-
3.108	002	111	2.495	-	200	2.958	002	111
3.299	100	-	2.704	101	-	3.124	100	-
			2.888	002	111			
			3.065	100	-			

Table S3. Percentage of phases observed in neutron diffraction data of H_2 dosed TE7 and OLC at low temperatures. Calculated percentages and ratios from integrating intensities under all peaks are displayed as Bank 3 | Bank 5

Sample	Pressure (Bar)	Temperature (K)	HCP H_2 phase (%)	FCC H_2 phase (%)	Al sample holder (%)	FCC : HCP
TE7	200	10	0.03 | 0.04	0.14 | 0.19	99.83 | 99.77	4.66:1 | 4.75:1
	200	15	0.08 | 0.09	0.00 | 0.00	99.92 | 99.91	0:1 | 0:1
	2000	10	0.22 | 1.15	0.25 | 1.35	99.53 | 97.50	1.14:1 | 1.17:1
	2000	15	0.23 | 1.13	0.25 | 1.26	99.52 | 97.61	1.09:1 | 1.12:1
	2000	25	0.22 | 1.12	0.24 | 1.27	99.54 | 97.61	1.09:1 | 1.13:1
OLC	2000	10	0.25 | 0.43	0.07 | 0.13	99.68 | 99.44	0.28:1 | 0.30:1
	2000	25	0.25 | 0.42	0.04 | 0.07	99.71 | 99.51	0.16:1 | 0.17:1

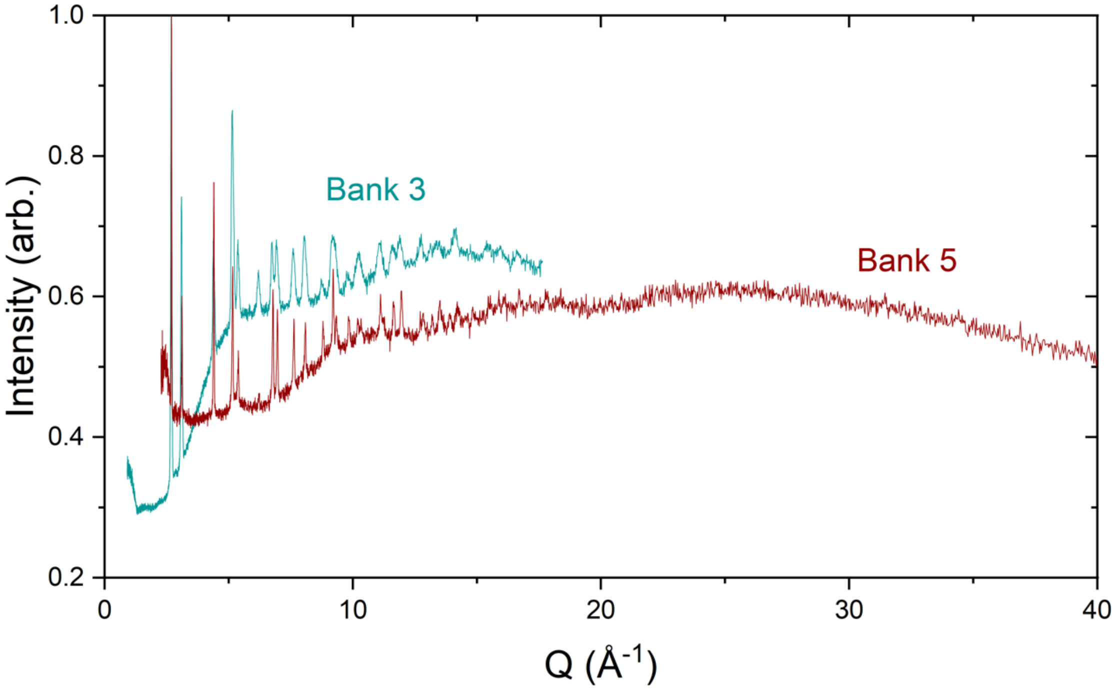

Figure S7: Diffraction of H_2 adsorbed in microporous TE7 at 2 kbar, 77 K plotted in momentum transfer (Q) units showing oscillations in the background signal. If diffuse scattering was coming from short-range ordering of hydrogen molecules, the background oscillations should match at the same Q value.

Table S4. Refined unit cell dimensions for HCP and FCC H_2 solids confined in TE7 and OLC porous carbons across the range of pressures and temperature observed. Full Rietveld analysis was conducted using TOPAS v6-Academic software.

		Microporous TE7					**Mesoporous OLC**	
Crystal system	Unit cell parameters	200 bar H_2		2 kbar H_2			2 kbar H_2	
		10 K	*15 K*	*10 K*	*15 K*	*25 K*	*10 K*	*25 K*
HCP	*a (Å)*	3.786(4)	3.769(3)	3.514(1)	3.515(9)	3.514(8)	3.598(3)	3.599(2)
	c (Å)	6.200(1)	6.150(6)	5.732(4)	5.736(3)	5.731(3)	5.869(8)	5.868(6)
	c/a	1.637	1.632	1.631	1.632	1.631	1.631	1.630
	Volume (Å^3)	76.9(2)	75.7(1)	61.31(6)	61.38(5)	61.3(4)	65.8(1)	65.8(1)
	Molar Volume^a (cm^3 /mol)	23.169	22.776	18.459	18.476	18.459	19.820	19.820
	Density^a (g/cm^3)	0.0870	0.0885	0.1092	0.1091	0.1092	0.1017	0.1017
FCC	*a (Å)*	5.364(3)	-	4.970(8)	4.970(6)	4.967(5)	5.084(5)	5.065(7)
	Volume (Å^3)	154.3(3)	-	122.77 (6)	122.77 (4)	122.54 (4)	131.4(4)	129.9(5)
	Molar Volume^b (cm^3 /mol)	23.222	-	18.476	18.476	18.442	19.781	19.550
	Density^b (g/cm^3)	0.0868	-	0.1091	0.1091	0.1093	0.1019	0.1031

^{a}HCP unit cell formula units $Z = 2$

^{b}FCC unit cell formula units $Z = 4$

Table S5. Refined unit cell dimensions for confined HCP and FCC H_2 solids observed via neutron diffraction at 10 K in this experiment compared to unit cell parameters taken from references[1-3].

		Confined H_2			**Bulk HCP**		**Bulk FCC**
		TE7 + H_2		OLC + H_2	Calculated[3]		Experiment[1,2]
Crystal system	Unit cell parameters	*10 K* *200 bar*	*10 K* *2 kbar*	*10 K* *2 kbar*	*11.92 K 187 bar*	*10.18 K 2.03 kbar*	*1.3 K* *1 bar*
HCP	*a (Å)*	3.786(4)	3.514(1)	3.598(3)	-	-	-
	c (Å)	6.200(1)	5.732(4)	5.869(8)	-	-	-
	c/a	1.637	1.631	1.631	-	-	-
	Volume ($Å^3$)	76.9(2)	61.31(6)	65.8(1)	-	-	-
	Molar Volume^a (cm^3 /mol)	23.169	18.459	19.820	*21.50*	*16.30*	-
	Density^a (g/cm^3)	0.0870	0.1092	0.1017	-	-	-
FCC	*a (Å)*	5.364(3)	4.9700(8)	5.084(5)	-	-	*5.312*
	Volume ($Å^3$)	154.3(3)	122.77(6)	131.4(4)	-	-	*149.891*
	Molar Volume^b (cm^3 /mol)	23.222	18.476	19.781	-	-	*22.567*
	Density^b (g/cm^3)	0.0868	0.1091	0.1019	-	-	*0.0893*

^{a}HCP unit cell formula units $Z = 2$

^{b}FCC unit cell formula units $Z = 4$

When comparing the molar volumes of the nanoconfined crystal phases to the bulk solids at similar temperatures (~10 K) and pressures (~200 and 2000 bar)[1-3]. In general, a larger volume was found for the confined phases. For HCP H_2 confined in the highly microporous TE7 at 200 bar and 2 kbar, the molar volume was 8% and 13 % larger than the equivalent bulk, respectively, and HCP-H_2 confined in mesoporous OLC at 2 kbar, having molar volumes 22% larger than the calculated bulk. For the observed FCC H_2 phase, the results were compared to the known unit cell molar volumes observed by Mills *et al*[1,2], while noting that these were recorded under significantly different pressure and temperature conditions (1.3 K, 1 bar) - as the FCC H_2 phase has not been observed at 10 K before. The results show that FCC H_2 confined in microporous TE7 at 200 bar, 10 K has a 3% larger molar volume than that observed in bulk FCC H_2 (1.3 K, 1 bar). Noting that the molar volume of bulk HCP decreases by ~24% with increasing pressure, it is reasonable to assume that the molar volume of FCC H_2 would follow a similar trend, thus FCC H_2 in TE7 at 2 kbar is likely still larger than the bulk FCC H_2 molar volume at the same pressure, if it formed at this temperature in the bulk.

The comparatively lower density than the bulk may be a function of the extremely high pressure used in this experiment. Similar results are seen for CO_2 sequestered in coal, whereby above a threshold pressure, the density of the confined phase becomes less than the bulk.[4] This may relate to the "break-even" threshold pressure observed in H_2 storage materials[5], and the flexibility of the porous substrate used. Lower pressure diffraction studies are required to confirm this hypothesis.

Table S6. Rotational peak parameters from the $J = 0 \rightarrow 1$ and $J = 1 \rightarrow 0$ transitions and the calculated mean squared displacements of each individual peak.

Adsorbed species	Temperature (K)	Peak Position (meV)	Peak height	Peak area[a]	FWHM	Transition (*J*,*m*)	$\langle U^2 \rangle$ (Å^2)
***Ortho*-H_2**	40	-14.7	6.7	210	5.0	1 > 0	0.26
		-13.3	15.2	318	5.0	1,±1 > 0,0	0.33
		-8.3	12.9	372	5.0	1,0 > 0,0	0.24
	4	-13	7.02	429	4.9	1,±1 > 0,0	0.31
		-8.3	14.6	291	4.6	1,0 > 0,0	0.24
***Para*-H_2**	40	17.1	63	202	2.4	0,0 > 1,0	0.34
		14.5	483	1414	2.4	0 > 1	0.44
		13.0	126	404	2.4	0,0 > 1,±1	0.35
	4	16.9	113	295	2.0	0,0 > 1,0	0.36
		14.5	1381	3779	2.0	0 > 1	0.34
		12.8	245	652	2.0	0,0 > 1,±1	0.27

[a] Peak areas corrected for spin-dependent incoherent scattering cross-sections[6]

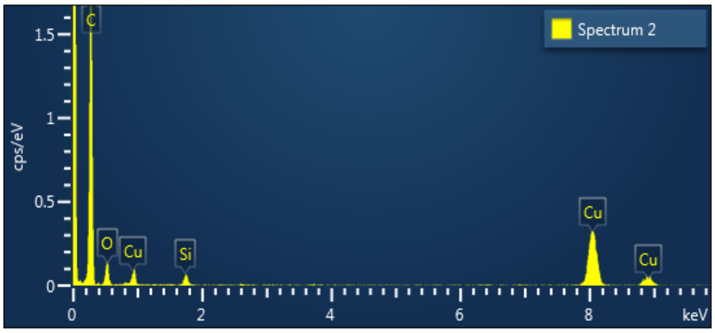

Figure S8. STEM EDX analysis of microporous TE7 after acid wash pretreatment. Revealing no trace metals or residual chlorine in the sample. Copper, silicon and oxygen were observed due to the copper TEM grid, silicon oxide grease contamination in the STEM and adsorbed water in the hygroscopic pores from sample transfer in air.

Table S7. The average parts per billion (ppb) and standard deviation (SD) of possible trace metals as reported by ICP-OES measurements in TE7 samples after acid washing.

Trace metal	average ppb	Average SD
Co	0.94	0.66
Fe	51.55	1.89
Mn	0.42	0.22
Cu	35.52	0.94

Table S8: Calculated percentage distribution of *para* and *ortho*-H_2 across the various adsorption sites of microporous TE7

Temperature (K)	H_2	Total (%)	>1 nm pore (%)	<1 nm pore (%)	Micropore site 2 (%)	Micropore site 3 (%)
4	**Total**	-	69	31	25	6
	Para	87	100	43	69	0
	ortho	13	0	57	31	100
40	**Total**	-	56	44	32	13
	Para	69	87	47	66	0
	ortho	31	13	53	34	100

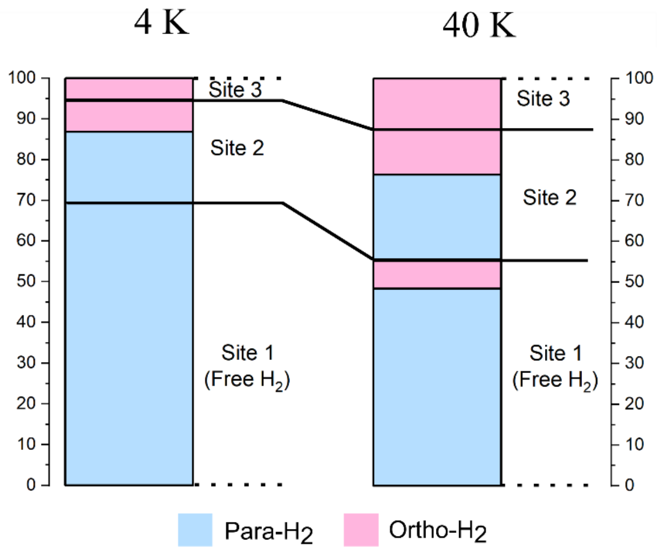

Figure S9: Percentage distribution of *para* and *ortho*-H_2 found in micropores < 1 nm (site 2 & 3) and in pores > 1 nm (site 1) of microporous TE7 at 40 and 4 K, 1 bar normal H_2

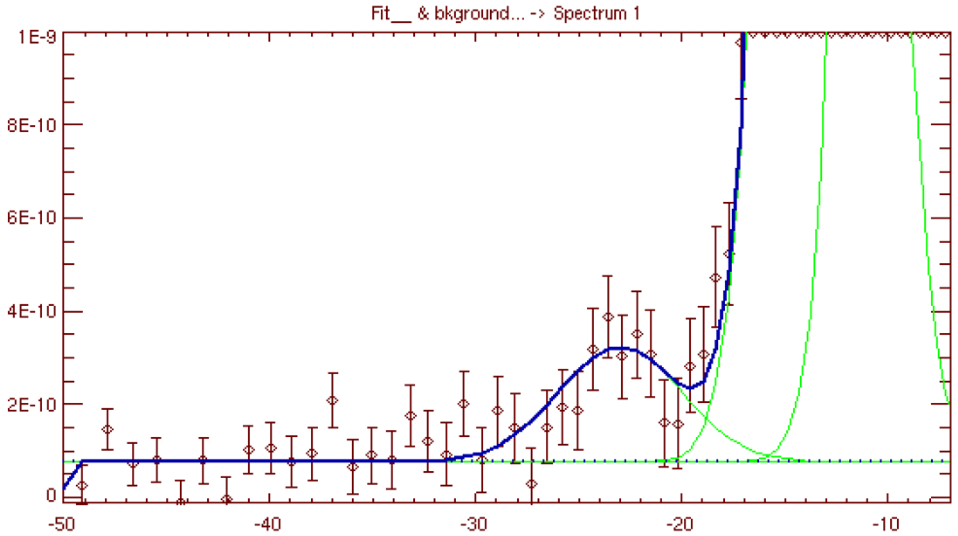

Figure S10: Inelastic neutron scattering of H_2 confined in TE7 at 4K. Gaussian fitting of a minute contribution to the neutron energy gain spectrum at -23 meV, closely corresponding to the projected transition (1,+/-1) -> (0,0) for a 1D vibrator at site (3).

Supplementary Information References

[1] A. F. Schuch, R. L. Mills, D. A. Depatie, Phys. Rev. 1968, 165, 1032.

[2] R. L. Mills, A. F. Schuch, Phys. Rev. Lett. 1965, 15, 722.

[3] A. Driessen, I. F. Silvera, J. Low Temp. Phys. 1984, 54.

[4] K. Yang, X. Lu, Y. Lin, A. V. Neimark, J. Geophys. Res. Solid Earth 2011, 116, 1.

[5] J. E. Sharpe, N. Bimbo, V. P. Ting, B. Rechain, E. Joubert, T. J. Mays, Microporous Mesoporous Mater. 2015, 209, 135.

[6] S. Mamone, M. Jiménez-Ruiz, M. R. Johnson, S. Rols, A. J. Horsewill, Phys. Chem. Chem. Phys. 2016, 18, 29369.

[7] S.-C. Lim, J. Lee, H. H. Kwak, J. W. Heo, M. S. Chae, D. Ahn, Y. H. Jang, H. Lee, S.-T. Hong, Exp. Cryst. Struct. Determ. 2017, DOI 10.5517/CCDC.CSD.CC1P42TQ.